Observation of Huge Surface Hole Mobility in the Topological Insulator $Bi_{0.91}Sb_{0.09}$ (111)

Dong-Xia Qu,* Sarah K. Roberts, and George F. Chapline
Lawrence Livermore National Laboratory, Livermore, California 94550, USA
(Received 18 April 2013; published 21 October 2013)

We report the first direct measurement of transport properties of surface states in the topological insulator $Bi_{0.91}Sb_{0.09}$ (111) from the weak-field Hall effect and Shubnikov–de Haas oscillations. We find that the holelike surface band displays an unexpectedly high mobility 23 000–85 000 $cm^2/V\,s$, which is the highest mobility so far reported in bismuth-based topological insulators. This result provides the first quantitative assessment of the effect of alloy disorder on the mobility of surface states in topological insulators. We show that the 9% alloy disorder decreases the mobility of surface states by a factor of less than 2.3.

DOI: 10.1103/PhysRevLett.111.176801 PACS numbers: 73.20.At, 71.18.+y, 73.25.+i, 75.47.−m

Topological insulators (TIs) are a newly discovered state of matter characterized by a nontrivial topological quantum number, which gives rise to an odd number of surface bands crossing the Fermi level between two time-reversal invariant momenta [1–5]. Unlike ordinary states of matter, these two-dimensional surface states are highly protected from disorder as a consequence of their chiral spin texture. The alloy $Bi_{1-x}Sb_x$ is the first discovered three-dimensional TI with five Fermi-level-crossed surface bands [6–9]. Later, the stoichiometric crystal Bi_2X_3 (X = Se and Te) was found to be a TI with a single Dirac cone [10–12]. It has been widely assumed that the surface transport mobility of Bi_2X_3 is, in principle, higher than that of $Bi_{1-x}Sb_x$, because the stoichiometric compounds usually have less disorder than an alloy like $Bi_{1-x}Sb_x$ [13]. However, the degree of mobility reduction due to random alloying has not yet been determined. Indeed, it is unclear whether the contribution of alloying perturbations to mobility reduction is greater than or less than the impact of scattering from charged defects [14,15]. Resolving this issue is therefore critical for both understanding the fundamental properties of surface states and also for optimizing the crystal growth method to use these states for spintronic devices and quantum computing applications.

Here, we report the first direct measurement of transport properties of surface states on the (111) surface of $Bi_{0.91}Sb_{0.09}$ via the weak-field Hall effect and Shubnikov–de Haas oscillations. We show that the mobility of the surface hole band can exceed 80 000 $cm^2/V\,s$, which is the highest mobility so far reported in three-dimensional TIs. We attribute this high mobility primarily to the reduction of the bulk charge density (6.8×10^{16} cm^{-3}), which is 18 times lower than the value of nonmetallic Bi_2Te_3. Our results demonstrate that the 9% alloy disorder reduces the electrical mobility of surface states by less than a factor of 2.3. We discuss other scattering mechanisms that might be of relevance in this material system.

A limitation of the TI Bi_2X_3 is the *aging effect*, or the time-dependent reconstruction of surface structures [16]. In contrast, the surface electronic states in $Bi_{1-x}Sb_x$ are naturally insensitive to the structural variation, owing to the fact that its surface band structure is robust against a wide range of Sb substitution ($0.07 < x < 0.18$) [17,18]. The surface states in the Bi-Sb system are hence expected to be immune to the time-dependent change of surface morphology. This feature suggests that the surface transport is more stable and controllable in the Bi-Sb alloy than in other bismuth-based TIs.

Previous transport and magnetic-optical measurements show that probing the surface conduction on the (111) surface of $Bi_{1-x}Sb_x$ is very difficult, because of not only the complicated surface band structure, but also the presence of surface states on other crystal planes [19–21]. For example, low-field magnetotransport measurements have only found an electron Fermi pocket on the $(2\bar{1}\,\bar{1})$ surface of $Bi_{1-x}Sb_x$, but cannot identify electronic states on the (111) surface [19]. The existence of locally flat minisurfaces was believed to produce the $(2\bar{1}\,\bar{1})$ surface conduction in these measurements.

To avoid current-carrying surface conduction on other crystal planes, single crystals $Bi_{1-x}Sb_x$ studied here were grown by the modified Bridgman method [22] and the samples were cleaved along the trigonal (111) plane without forming micrometer scale terraces. Figure 1(a) shows the Fermi surface map of $Bi_{0.91}Sb_{0.09}$ (111) in the surface Brillouin zone, which consists of a Dirac surface band enclosing the $\bar{\Gamma}$ point, six hole pockets in between $\bar{\Gamma}$ and $\bar{M}$, and six electron pockets near the $\bar{M}$ point. Spin-sensitive angle-resolved photoemission spectroscopy (ARPES) measurements have demonstrated that the Dirac band and the hole pocket form a Kramers pair by spin-orbit interaction [Fig. 1(b)] [9]. In particular, if we can tune the Fermi level close to the bulk valence band, the holelike surface band may dominate surface conduction, making it more accessible in transport experiments than the other two electron bands.

In this study, we use $Bi_{0.91}Sb_{0.09}$ crystals with the Fermi level inside the bulk band gap. As shown in Fig. 1(c), the

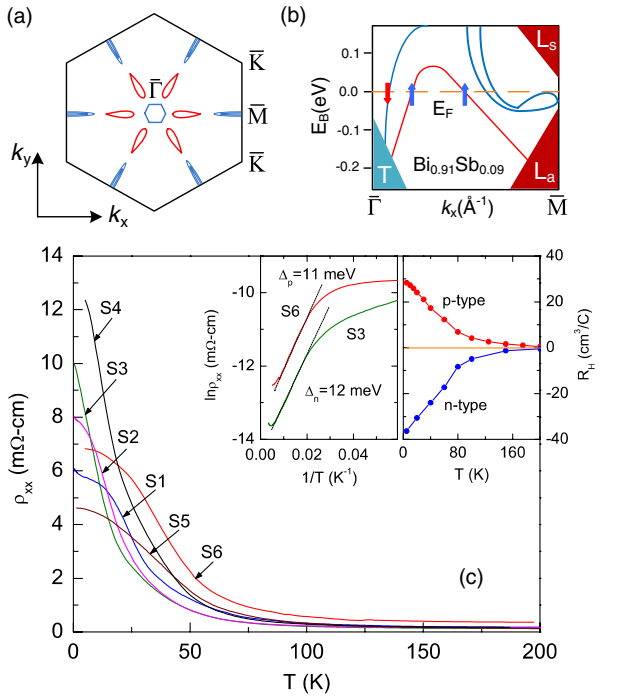

FIG. 1 (color online). (a) Sketch of the (111) surface Brillouin zone with a hexagonal electron pocket around $\bar{\Gamma}$, six tear-shaped hole pockets along the $\bar{\Gamma}$-$\bar{M}$ direction, and six bowtie-shaped electron pockets around $\bar{M}$. The $\bar{\Gamma}$, $\bar{M}$, and $\bar{K}$ are high symmetry points. (b) Surface band structure along the $\bar{\Gamma}$-$\bar{M}$ direction mapped by ARPES experiments in $Bi_{0.91}Sb_{0.09}$ (111) (traced from [8,9]). The spin direction of each band is marked by the arrows. (c) The resistivity ρ_{xx} vs temperature T for samples $S1$–$S6$ between 4 and 200 K. The left panel of the insets shows the Arrhenius plot of $\ln\rho_{xx}$ vs $1/T$ for the n-type sample $S3$ and p-type sample $S6$. The right panel shows the Hall coefficient R_H vs T for representative n- and p-type samples.

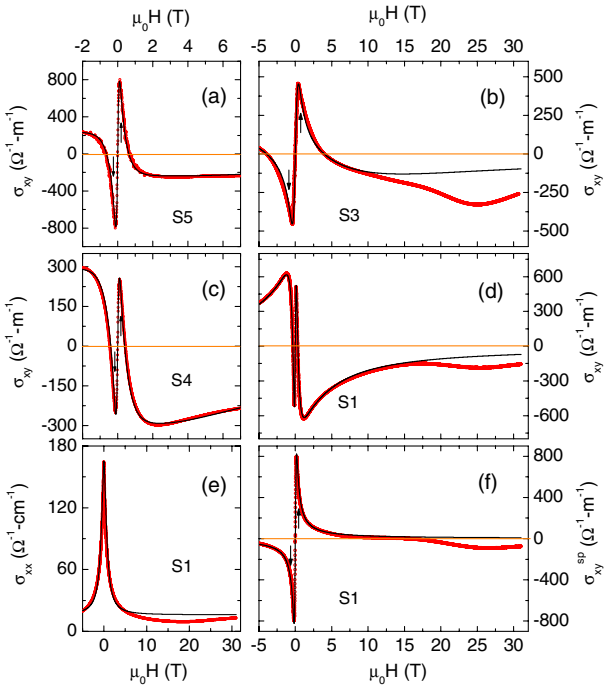

FIG. 2 (color online). (a)–(d) The Hall conductivity σ_{xy} vs H for samples $S5$, $S3$, $S4$, and $S1$ (red circles). The solid line is the fit to σ_{xy} in Eq. (1). Arrows indicate the peak field B_p, which is related to the mobility by $\mu_{sp} = 1/B_p$. (e) The conductivity σ_{xx} measured with H at 0.3 K for sample $S1$ (red circles). The solid curve is the calculated σ_{xx} from Eq. (1) with a bulk mobility $\mu_b = 13\,000$ cm^2/V s. (f) The holelike surface Hall conductivity σ_{xy}^{sp} vs H, obtained by subtracting the bulk term σ_{xy}^{b} and electronlike surface Hall conductivity σ_{xy}^{sn} at $T = 0.3$ K for sample $S1$. The solid curve is the fit to Eq. (2).

resistivity ρ_{xx} in samples $S1$–$S6$ steeply increases by almost 2 orders of magnitude when the temperature T is lowered from 200 to 4 K. As determined from the sign of the Hall resistivity ρ_{yx}, samples $S1$–$S5$ are n-type, whereas sample $S6$ is p-type. The Arrhenius plot of ρ_{xx} in samples $S1$ and $S6$ indicates a thermal activation behavior with an activation gap $\Delta = 12$ and 11 meV, respectively. Moreover, the Hall coefficient R_H in the n- and p-type samples exhibits similar magnitudes [Fig. 1(c), right panel of the insets], indicating that the electron bulk conduction and hole bulk conduction are comparable and compensated.

In the n-type samples, we observe a pronounced weak-field Hall anomaly. As shown in Figs. 2(a)–2(e), the measured Hall conductivity σ_{xy} (red dots) is plotted for five different samples, $S1$–$S5$, in which the applied magnetic field H changes σ_{xy} from holelike to electronlike at $H <$ 1 T. This dispersive anomaly dominates the low-H Hall conduction in accordance with a high mobility band that is p-type. The amplitude of the Hall anomaly rapidly decreases as T is increased from 0.3 to 21 K [inset of Fig. 3(a) and see Ref. [23] for details]. This effect is similar to what has been found in the TI Bi_2Te_3, where a much smaller n-type Hall anomaly was observed in a p-type crystal and was confirmed to originate from surface states [12]. We may rule out the possibility that the low-H holelike conduction arises from the bulk band. If we interpreted the observed $\sigma_{xy}(B)$ as the sum of two bulk conductivity with the opposite sign, the carrier density of each band would be $\approx 10^{15}$ cm^{-3}. Then we would have a bulk resistivity, e.g., in sample $S5$, $\rho_{xx} = 42$ mΩ cm, which is more than 10 times higher than the observed resistivity. The observation of a low-H Hall anomaly therefore indicates the existence of a p-type channel that is most likely coming from the surface.

We next fit the observed Hall conductivity as the sum of three conductivity tensors

$$\sigma_{ij} = \sigma_{ij}^{b} + \sigma_{ij}^{sp} + \sigma_{ij}^{sn}, \quad (1)$$

where σ_{ij}^{b} is the bulk conductivity, σ_{ij}^{sp} the p-type surface conductivity, and σ_{xy}^{sn} the n-type surface conductivity. With $\sigma_{ij}^{s} = G_{ij}^{s}/t$ (t is the sample thickness), G_{xy}^{s} corresponds to the surface Hall conductance given by

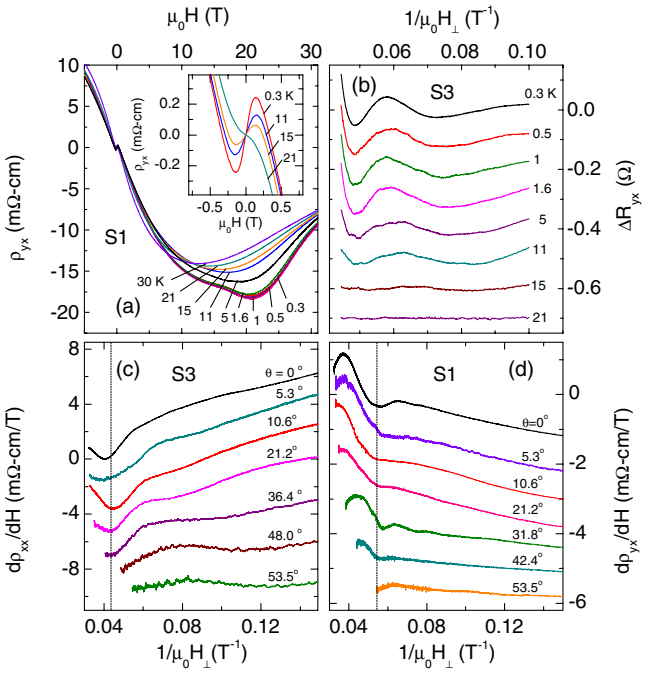

FIG. 3 (color online). (a) The trace of the Hall resistivity ρ_{yx} vs H in sample $S1$ measured at temperature T between 0.3 and 30 K. The inset shows that the amplitude of the weak-field Hall anomaly decreases rapidly as T is raised from 0.3 to 21 K. (b) ΔR_{yx} vs $1/H$ obtained by subtracting a smooth background at selected T in sample $S3$. (c) The resistivity derivative $d\rho_{xx}/dH$ vs $1/H_\perp$ with $H_\perp = H\cos\theta$ at selected tilt angles θ in sample $S3$. (d) The Hall resistivity derivative $d\rho_{yx}/dH$ vs $1/H_\perp$ at various θ in sample $S1$.

$$G^s_{xy} = g_i \frac{2\pi e^3}{h^2} \frac{Bl^2}{[1 + (\mu_s B)^2]}, \qquad (2)$$

where g_i is the degeneracy of the surface band i ($g_i = 6$ for the holelike band), l the mean free path, h Planck's constant, e the electron charge, and μ_s the surface Hall mobility, which is related to the metallicity parameter $k_F l$ as $\mu_s = el/\hbar k_F$. We can achieve a very close fit to the observed σ_{xx} and σ_{xy} by Eq. (1) in all five samples at low fields [solid lines, Figs. 2(a)–2(d)]. In Fig. 2(f), the calculated p-type surface term in $S1$ is plotted in a solid curve, which well captures the profile of the isolated surface conductivity (plotted in red circles and obtained by subtracting $\sigma^b_{xy} + \sigma^{sn}_{xy}$ from the observed σ_{xy}). Table I summarizes the parameters for five samples that all display a weak-H Hall anomaly. The extracted surface hole band mobility can reach 85 000 $\mathrm{cm}^2/\mathrm{V\,s}$, which is even higher than the electron mobility (34 000 $\mathrm{cm}^2/\mathrm{V\,s}$) in the strained HgTe three-dimensional TI [24].

To find out whether such a high mobility surface state will be quantized into Landau energy levels in the presence of a magnetic field, we measured two samples both showing a low-H Hall anomaly at magnetic fields up to 31 T. This field is far above the quantum limit of bulk carriers [23]. As shown in Fig. 3(a), the raw trace of the Hall resistivity ρ_{yx} displays weakly resolved oscillations sitting on top of a strongly nonlinear background for fields exceeding 10 T. The oscillations are more pronounced when a smooth background is subtracted [Fig. 3(b)]. As T is raised from 0.3 to 21 K, the oscillation amplitudes decrease quickly, accompanied by the decrease of the Hall anomaly [inset of Fig. 3(a)]. Figures 3(c) and 3(d) plot the derivative $d\rho_{xx}/dH$ and $d\rho_{yx}/dH$ vs the perpendicular field component $H_\perp = H\cos\theta$ along the trigonal axis [111] (θ is the tilting field relative to the trigonal axis), for samples $S3$ and $S1$, respectively. For both samples, the most pronounced dip (marked by dashed lines) depends only on $H_\perp$, and they are absent for $55° \leq \theta \leq 90°$. This distinctive behavior is a direct evidence of the surface origin of the high-H quantum oscillations.

Figure 4(a) shows the traces of $\rho_{yx}(H)$ and $\rho_{xx}(H)$ vs H for sample $S3$ at 0.3 K. We find that the quantum oscillations are more prominent in $\rho_{yx}(H)$ than in $\rho_{xx}(H)$ (see Ref. [23] for detailed discussion). To extract the period of the oscillations, we plot the Landau fan diagram using the extrema of $d\rho_{xx}/dH$ and $d\rho_{yx}/dH$ [Fig. 4(b)] for sample $S3$ in Fig. 4(c). It can be seen that all the data lie

TABLE I. Parameters in samples $S1$, $S2$, $S3$, $S4$, and $S5$. The dimension of the sample $L \times W \times t$ (length, width, thickness) is in units of μm. The uncertainties in measuring t is approximately $\pm 10\%$. μ_{sp} and n_{sp} correspond to the Hall mobility and lower bound of the carrier density of the holelike surface state, respectively (see Ref. [23] for details). S_F, k_F, and $k_F l$ are the lower bound of Fermi surface cross section, average wave vector, and metallicity parameter of the p-type surface state, respectively. All these values are obtained from fitting measured $\sigma_{xy}(H)$ and $\sigma_{xx}(H)$ to Eq. (1).

Units	$L \times W \times t$ μm^3	μ_{sp} m^2/V s	n_{sp} 10^{12} cm^{-2}	S_F T	k_F (Å^{-1})	$k_F l \cdots$
$S1$	825 × 170 × 30	6.0	5.30	18.3	0.024	220
$S2$	350 × 170 × 20	8.0	1.80	6.21	0.013	95
$S3$	880 × 390 × 40	2.3	10.8	37.3	0.034	162
$S4$	600 × 300 × 30	8.0	1.48	5.10	0.012	75
$S5$	840 × 270 × 50	8.5	6.28	21.7	0.026	368

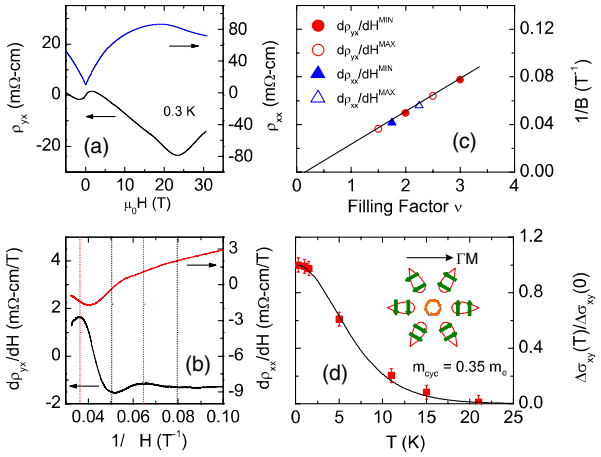

FIG. 4 (color online). (a) ρ_{xx} and ρ_{yx} vs H in sample $S3$ at 0.3 K. (b) The high-field quantum oscillations in the plot of $d\rho_{xx}/dH$ and $d\rho_{yx}/dH$ vs $1/H$. Black and red dashed lines correspond to the minima and maxima of $d\rho_{yx}/dH$, which are phase shifted by $\pi/2$ from the extrema of $d\rho_{xx}/dH$. (c) The Landau level index plot using the extrema of $d\rho_{xx}/dH$ and $d\rho_{yx}/dH$. The minima of $d\rho_{yx}/dH$ identify the fields corresponding to the filling factor ν, while the minima of $d\rho_{yx}/dH$ correspond to $\nu - \frac{1}{4}$ [23]. (d) The normalized Hall conductivity amplitude $\Delta\sigma_{xy}(H)/\Delta\sigma_{xy}(0)$ vs T at 0.3 K with 15 T. The fit to the Lifshitz-Kosevich expression gives $m_{cyc} = 0.35m_e$. The inset shows the spin texture with arrows pointing to the spin direction, as revealed by ARPES measurements.

on a straight line that intersects the ν axis at 0.15, suggesting a conventional Schrödinger spectrum. The slope of the extrapolated straight line gives $S_F = 36.0$ T, with an average Fermi wave vector $k_F = 0.033$ Å^{-1}. These values are in good agreement with the parameters of the p-type surface state estimated from the Hall anomaly analysis (Table I and Sec. S3 in Ref. [23]).

By fitting the T dependence of the Hall conductivity amplitudes to the standard Lifshitz-Kosevich expression [Fig. 4(d)], we get the cyclotron mass $m_{\rm cyc} = 0.35m_e$ in sample $S3$ (m_e is the free electron mass). With $k_F = 0.033$ Å^{-1}, the average Fermi velocity ($v_F = \hbar k_F/m_{\rm cyc}$) is found to be 1.1×10^5 m/s. This number is closer to the ARPES observed average value of 2.5×10^5 m/s for the hole surface band ($v_F \sim 0.76$ and 4.3×10^5 m/s along the k_x and k_y directions, respectively) than 3.7 and 4.9×10^5 m/s for the electron surface bands surrounding the $\bar{\Gamma}$ and $\bar{M}$ points, respectively [8]. This fact, together with the Hall anomaly analysis, makes us conclude that the observed quantum oscillations are coming from the p-type surface state.

Interestingly, despite the strong alloying, the magnitude of surface mobility in the best $Bi_{0.91}Sb_{0.09}$ sample is 8 times higher than that of stoichiometric crystal Bi_2Te_3 (10 000 cm^2/V s) [12,25]. At low temperatures, the final transport mobility is determined by the scattering from disorder, which includes structural disorder and charge disorder. The charge disorder has been identified as the primary source of bulk carrier doping in bismuth-based bulk TIs [26,27]. We hence attribute the increase of μ_s in $Bi_{0.91}Sb_{0.09}$ to the significant reduction of scattering from the charge disorder. In fact, the bulk carrier concentration of $Bi_{0.91}Sb_{0.09}$ is 18 times smaller than that of Bi_2Te_3 (1×10^{18} cm^{-3}). If there were no alloy disorder and interband scattering in $Bi_{0.91}Sb_{0.09}$ [inset of Fig. 4(d)], the μ_s of $Bi_{0.91}Sb_{0.09}$ would get to 1.8×10^5 cm^2/V s as compared to Bi_2Te_3. The observation of 8 times enhancement in μ_s indicates that the upper bound on the reduction of mobility due to alloy disorder is less than 43%. This phenomenon is consistent with the unique characteristic of surface states in a TI, in which backscattering caused by atomic scale disorder is absent between states of opposite spin [28]. Furthermore, although the holelike bands are irrelevant to the topological quantum number, they are still indirectly protected against surface defects by interband scattering, i.e., the scattering between the Dirac band that carries a nonzero Berry's phase and surface hole bands [29]. In contrast, the spin-polarized surface states in pure Bi (111), however, do not support a nonzero Berry's phase because the time-reversal invariant momenta are enclosed an even number of times [6]. These nontopological surface states can still be localized by scattering from surface defects.

In conclusion, we have obtained the first time experimental measurement of the transport properties of surface states in $Bi_{0.91}Sb_{0.09}$ (111) from the weak-field Hall anomaly and Shubnikov–de Haas oscillations. We show that the surface band exhibits a surprisingly high mobility 23 000–85 000 cm^2/V s despite a high level of alloy disorder. This result provides the first quantitative analysis of the degree of mobility reduction due to random alloying in a TI. Given the fact that Bi-Sb system is more stable than Bi_2X_3 compounds, these spin-polarized surface states are potentially more useful for realizing spin-based devices that rely on high electrical mobility.

We would like to thank H.-J. Zhang and S.-C. Zhang for helpful discussions. The high magnetic field measurements were performed at the National High Magnetic Field Laboratory, Tallahassee, Florida. We would like to thank D. Graf, A. Suslov, and G. S. Boebinger for assistance with the experimental measurements. This work was supported by LDRD (12-ERD-027) from Lawrence Livermore National Laboratory.

*dxqu@lbl.gov

[1] C. L. Kane and E. J. Mele, Phys. Rev. Lett. **95**, 146802 (2005).
[2] B. A. Bernevig and S.-C. Zhang, Phys. Rev. Lett. **96**, 106802 (2006).
[3] J. E. Moore and L. Balents, Phys. Rev. B **75**, 121306(R) (2007).

[4] M. Z. Hasan and C. L. Kane, Rev. Mod. Phys. **82**, 3045 (2010).
[5] X.-L. Qi and S.-C. Zhang, Rev. Mod. Phys. **83**, 1057 (2011).
[6] L. Fu and C. L. Kane, Phys. Rev. B **76**, 045302 (2007).
[7] J. C. Y. Teo, L. Fu, and C. L. Kane, Phys. Rev. B **78**, 045426 (2008).
[8] D. Hsieh, D. Qian, L. Wray, Y. Xia, Y. S. Hor, R. J. Cava, and M. Z. Hasan, Nature (London) **452**, 970 (2008).
[9] D. Hsieh *et al.*, Science **323**, 919 (2009).
[10] Y. Xia *et al.*, Nat. Phys. **5**, 398 (2009).
[11] H. Zhang, C.-X. Liu, X.-L. Qi, X. Dai, Z. Fang, and S.-C. Zhang, Nat. Phys. **5**, 438 (2009).
[12] D.-X. Qu, Y. S. Hor, J. Xiong, R. J. Cava, and N. P. Ong, Science **329**, 821 (2010).
[13] E. J. Moore, Nat. Phys. **5**, 378 (2009).
[14] D. Kim, S. Cho, N. P. Butch, P. Syers, K. Kirshenbaum, S. Adam, J. Paglione, and M. S. Fuhrer, Nat. Phys. **8**, 459 (2012).
[15] H. Beidenkopf, P. Roushan, J. Seo, L. Gorman, I. Drozdov, Y. S. Hor, R. J. Cava, and A. Yazdani, Nat. Phys. **7**, 939 (2011).
[16] X. He, W. Zhou, Z. Y. Wang, Y. N. Zhang, J. Shi, R. Q. Wu, and J. A. Yarmoff, Phys. Rev. Lett. **110**, 156101 (2013).
[17] H. Guo *et al.*, Phys. Rev. B **83**, 201104(R) (2011).
[18] A. Nishide, A. A. Taskin, Y. Takeichi, T. Okuda, A. Kakizaki, T. Hirahara, K. Nakatsuji, F. Komori, Y. Ando, and I. Matsuda, Phys. Rev. B **81**, 041309(R) (2010).
[19] A. A. Taskin and Y. Ando, Phys. Rev. B **80**, 085303 (2009).
[20] A. A. Taskin, K. Segawa, and Y. Ando, Phys. Rev. B **82**, 121302(R) (2010).
[21] A. A. Schafgans, K. W. Post, A. A. Taskin, Y. Ando, X.-L. Qi, B. C. Chapler, and D. N. Basov, Phys. Rev. B **85**, 195440 (2012).
[22] Y. S. Hor and R. J. Cava, J. Alloys Compd. **479**, 368 (2009).
[23] See Supplemental Material at http://link.aps.org/supplemental/10.1103/PhysRevLett.111.176801 for more experimental data and discussion.
[24] C. Brune, C. X. Liu, E. G. Novik, E. M. Hankiewicz, H. Buhmann, Y. L. Chen, X. L. Qi, Z. X. Shen, S. C. Zhang, and L. W. Molenkamp, Phys. Rev. Lett. **106**, 126803 (2011).
[25] D.-X. Qu, Y. S. Hor, and R. J. Cava, Phys. Rev. Lett. **109**, 246602 (2012).
[26] Y. S. Hor, D. Qu, N. P. Ong, and R. J. Cava, J. Phys. Condens. Matter **22**, 375801 (2010).
[27] R. J. Cava, H. Ji, M. K. Fuccillo, Q. D. Gibson, and Y. S. Hor, J. Mater. Chem. C **1**, 3176 (2013).
[28] P. Roushan, J. Seo, C. V. Parker, Y. S. Hor, D. Hsieh, D. Qian, A. Richardella, M. Z. Hasan, R. J. Cava, and A. Yazdani, Nature (London) **460**, 1106 (2009).
[29] J. Seo, P. Roushan, H. Beidenkopf, Y. S. Hor, R. J. Cava, and A. Yazdani, Nature (London) **466**, 343 (2010).